Three-Dimensional Printing of Porous Ceramic Scaffolds for Bone Tissue Engineering

Hermann Seitz, Wolfgang Rieder, Stephan Irsen, Barbara Leukers, Carsten Tille

Caesar Research Center, Rapid Prototyping Group, Ludwig-Erhard-Allee 2, 53175 Bonn, Germany

Received 25 September 2004; revised 10 January 2005; accepted 10 January 2005
Published online 24 June 2005 in Wiley InterScience (www.interscience.wiley.com). DOI: 10.1002/jbm.b.30291

Abstract: This article reports a new process chain for custom-made three-dimensional (3D) porous ceramic scaffolds for bone replacement with fully interconnected channel network for the repair of osseous defects from trauma or disease. Rapid prototyping and especially 3D printing is well suited to generate complex-shaped porous ceramic matrices directly from powder materials. Anatomical information obtained from a patient can be used to design the implant for a target defect. In the 3D printing technique, a box filled with ceramic powder is printed with a polymer-based binder solution layer by layer. Powder is bonded in wetted regions. Unglued powder can be removed and a ceramic green body remains. We use a modified hydroxyapatite (HA) powder for the fabrication of 3D printed scaffolds due to the safety of HA as biocompatible implantable material and efficacy for bone regeneration. The printed ceramic green bodies are consolidated at a temperature of 1250°C in a high temperature furnace in ambient air. The polymeric binder is pyrolysed during sintering. The resulting scaffolds can be used in tissue engineering of bone implants using patient-derived cells that are seeded onto the scaffolds.This article describes the process chain, beginning from data preparation to 3D printing tests and finally sintering of the scaffold. Prototypes were successfully manufactured and characterized. It was demonstrated that it is possible to manufacture parts with inner channels with a dimension down to 450 μm and wall structures with a thickness down to 330 μm. The mechanical strength of dense test parts is up to 22 MPa.

Keywords: 3D printing; scaffolds; bone tissue engineering; hydroxyapatite; rapid prototyping

INTRODUCTION

Critical-size bone defects often result from trauma or tumors and cannot be repaired by the body. The application of synthetic bone replacement has a high clinical potential for filling these defects because bone grafts do not have to be harvested from donors or other places in the body. As a consequence, the risk of tissue rejection and disease transfer from donor tissue can be eliminated. Today, various synthetic materials for bone replacement are available. Normally, these materials are produced in simple geometries like blocks, pins, or splines. Rapid Prototyping and especially three-dimensional printing (3D printing) is well suited to generate complex porous ceramic matrices directly from powder materials. Furthermore, these technologies allow to manufacture bone grafts with complex shapes as well as designed internal channel networks to mimic bone structures. Anatomical information obtained from patients can be used to design and optimize the implant for a target defect. Then, the implant is manufactured straight from a 3D data set without a mold.

The matrices generated by 3D printing can be used for bone tissue engineering using patient-derived cells that are seeded onto the scaffolds. The scaffolds serve as 3D templates for initial cell attachment and subsequent tissue formation. The aim is to produce biocompatible scaffolds for bone replacement with fully interconnected channels.

Rapid prototyping, also known as solid free-form fabrication is a class of well-established techniques to manufacture prototypes from complex 3D datasets. All rapid prototyping processes are based on the same principle of building 3D models layer by layer. There are several rapid prototyping machines on the market, each having advantages and disadvantages. The most important techniques are stereolithography, fused deposition modeling, selective laser sintering, and 3D printing.[1] Today, prototype models are mainly used for engineering test and evaluation issues.

Due to the capability to fabricate complex 3D shapes with controlled internal structure, the use of rapid prototyping to generate scaffolds is a promising area. Several studies have investigated the application of various rapid prototyping tech-

Correspondence to: Hermann Seitz (e-mail: seitz@caesar.de)

Figure 1. Flexible 3D printing test setup used for process investigation.

nologies for the manufacturing of scaffolds for tissue engineering.[2] The materials used in RP processes are polymers, ceramics, and composites of polymers and ceramics. Biodegradable and bioresorbable polymeric and composite scaffolds with defined internal structures have been manufactured directly as well as indirectly using stereolithography (SLA),[3] fused deposition modeling,[4] 3D plotting,[5,6] and 3D printing.[7–10] Ceramic scaffolds for bone replacement have been produced using laminated object manufacturing,[11] selective laser sintering,[12] SLA,[13] and 3D printing.[14] Furthermore, wax molds generated by the ModelMaker II RP system (Solidscape Inc., USA) were also used to fabricate ceramic[15] and composite scaffolds.[16]

The aim of the current study was to investigate the capabilities of a ceramic-based process chain for the fabrication of porous scaffolds for bone tissue engineering. The main technology is the 3D printing technique that is used to manufacture ceramic green parts that are sintered afterwards. This technique has been chosen because scaffolds can be fabricated directly without a mold, various ceramic materials can be tested very easily, and the technique has the capability of manufacturing porous scaffolds with controlled internal structures with high resolution. Furthermore, the 3D printing process allows production of custom bone implants based on patients' datasets. The complete fabrication process, from data preparation and 3D printing tests to sintering of the scaffold is presented. To investigate the capabilities of the process chain, 3D test structures were successfully manufactured and characterized.

MATERIALS AND METHODS

A 3D printing test setup like shown in Figure 1 was used for process investigations. The machine was designed and built in cooperation with Generis GmbH (Augsburg, Germany). The essential elements of this device are two z-pistons, one acting as a powder reservoir and one as a building box, an x-y plotter for moving the printing device, the recoating unit, and several electronic control devices. The x-axis is defined as fast axis that moves the printing device bidirectional across the building box during printing. The slow y-axis moves the x-axis step by step. The machine features a relatively small building envelope of $100 \times 100 \times 100$ mm^3 to be able to test small amounts of powder materials. A microdispensing valve with a nozzle diameter of 76 μm was chosen to print binder solution on the powder bed. The valve features a wide range of fluid compatibility and was found to be the best for process investigations. The flexibility of the 3D printing setup makes it possible to investigate both new process techniques and new material combinations.

The process starts with a 3D dataset that is sliced by a computer to generate the printing matrix of each layer. The recoating mechanism carries an amount of ceramic powder from the powder reservoir to the building box, thereby creating a thin layer of powder on the top of the building box. The liquid binder is printed on the layer of powder using the microdispensing valve according to the current cross-section of the part. The ceramic powder is bonded in these selected regions. When the layer is completed, the building box piston moves down by the thickness of a layer and a new layer of

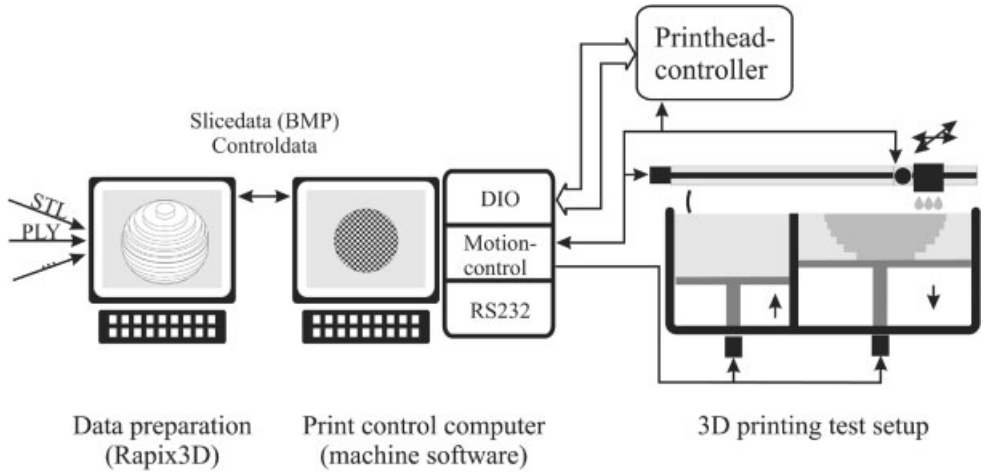

Figure 2. Process chain beginning from data preparation, process control to 3D printing.

powder is deposited on the first one. These process steps are repeated until the whole part is formed within the powder bed. The surrounding powder material supports the part during the building process. Thus, there is no need for support structures for features such as large overhangs and undercuts. After completion, the part is removed from the building box, cleaned using an air blower, and air dried. After that, the part is sintered for 2 h at a temperature of 1250°C in an electrically heated chamber furnace (Carbolite, Ubstadt-Weiher, Germany) in ambient air. The organic binder is removed during sintering by pyrolysis and the green body obtains its desired mechanical properties. The sintering also typically causes shrinkage of the ceramic green body.

The system of the process control form a 3D dataset to 3D printing is shown in Figure 2. The software Rapix3D (Forwiss Passau, Germany) is used on a Windows-based computer to prepare STL files for 3D printing. Rapix3D has a graphical user interface (GUI) that enables the user to load 3D STL-files or other data types like .ply and position it in a virtual building box. The software also allows basic data manipulations like rotation, translation, and automatic positioning. The loaded models are sliced by Rapix3D to generate the printing matrix of each layer at every z-level. After that, these images (BMP-format) are successively sent to a print control computer, which drives the axes of the 3D printer and the microdispensing valve. The print control computer features a four-axial motion control card to operate the servomotors of the pistons and of the x-y axes. The servomotor of the recoating unit is driven directly via serial connection. A high-speed digital IO card generates the signals for the microdispensing valve dependent on its actual x-y position and according to the printing matrix. A machine software was programmed in C++ (MFC), which receives the printing matrices from the data preparation computer and controls the complete printing process.

In some cases it is favorable to draw the bitmaps of the different slices manually. Simple graphic tools can be used to do this. These bitmap files can be imported into the machine software. This allows defining the actually printed bits of each layer. Consequently, test structures can be designed very precisely without rounding error, which can occur when slicing a 3D dataset. Especially, it is an easy method to generate two-and-a-half-dimensional (2.5D) models as an extrusion of one two-dimensional bitmap.

An important parameter of scaffolds for bone replacement is the compression strength of the material. Therefore, a first test structure was designed for mechanical tests. It is a simple cylinder with a diameter of 15 mm and a height of 30 mm. A second test structure shown in Figure 3 also features a cylindrical shape (11 mm diameter, 11.25 mm height) with regular channel structure. The channel structure has a square cross-section of 0.75×0.75 mm^2. This part was designed to test the ability to build small inner channels in a scaffold. The channel size is an important parameter because it determines cell infiltration and tissue ingrowth. A third test structure (Figure 4, left) with a narrow wall thickness of 0.4 mm was designed to test the possible structural resolution of the printing process. Because cancellous bone has a very fine microstucture, a high resolution of the process is necessary to mimic natural bone.

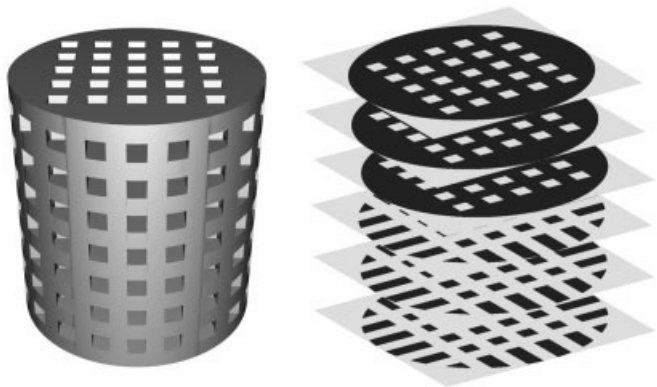

Figure 3. Schematic of the channel test part with regular quadratic channel structure. 3D rendering of the CAD file (left); exemplary illustration of six out of 45 layers (right) with two different printing matrices.

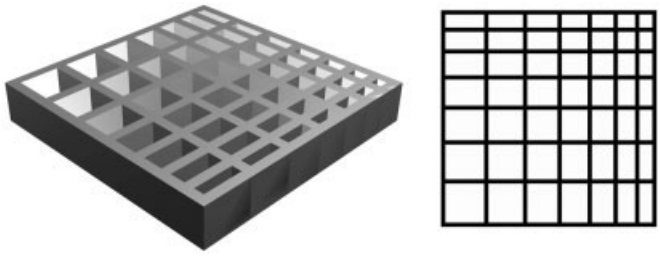

Figure 4. Grid test part with structural resolution of one pixel. (left: 3D rendering of the CAD model, right: printing matrix/bitmap of a single layer that was used to define the 2.5D models).

The volume of the droplets ejected from the microdispensing valve depends on the drive pulse parameters and the jetted fluid. The x-y printing raster resolution was 0.2 or 0.25 mm. The designed structures (e.g., cross-section of the channels, wall thickness of the grid structure) are multiples of the raster resolution to avoid rounding errors that can occur when calculating the printing matrix. The thickness of the powder layers is chosen 0.2, 0.25, or 0.3 mm, depending on the test part to be printed. The three test structures are hereinafter referred to as compression test part, channel test part, and grid test part. The printing parameters are listed in Table I for all test parts.

The compression test part was designed using the software Magics (Materialise, Belgium). The channel and grid test part were designed by drawing the bitmaps of the different slices utilizing the software graphic tool Corel Draw (Corel Corporation). The grid test part was defined by eight layers of a single bitmap (see Figure 4, right), whereas the channel test part consists of several layers of two different bitmaps (Figure 3, right).

Hydroxyapatite is a promising ceramic material to manufacture scaffolds for bone tissue engineering because the chemical composition is comparable to the inorganic part of native bone. From the process point of view, 3D printing requires a powder with good flowability, a controlled particle size distribution, and a suitable and strong binder interaction. Therefore, the spray-dried hydroxyapatite granulates with polymeric additives V5.2 and V12 (Friedrich-Baur-Institut, Bayreuth, Germany) were chosen for 3D printing tests. The polymeric binder Schelofix (Friedrich-Baur-Institut, Bayreuth, Germany) was dissolved in water (10 and 14 wt %) and used as binder fluid to be jetted by the microdispensing valve. To receive optimized printing results the printing parameter and materials have been adjusted depending on the test part to be printed (see Table 1). A detailed study about various materials that were previously tested on our 3D printing test setup will be reported soon (Irsen et al., unpublished).

Because 3D printing is a powder-based process where particles are glued together by a binder fluid, the resulting parts are not completely dense but feature a built-in microporosity.

Physical properties of the printed bodies like compression strength and pore diameter were determined. The compression strength of the compression test part was measured using a uniaxial testing system (Zwick GmbH & Co KG, Ulm, Germany). The geometric dimensions of the internal channels and the grid test part were measured optically. The shrinkage of scaffolds was determined by measuring the diameter and length of unsintered and sintered compression test parts using a sliding caliper. The 3D printed channel test parts have also been analyzed by SEM (Supra 55, Carl Zeiss NTS GmbH, Oberkochen, Germany) to characterize the porosity of the compact materials and the surface texture on a microscale.

RESULTS

Several specimens of the three test parts were successfully manufactured. The grid test parts were very fragile after printing and had to be handled very carefully. About 10% of these test parts were destroyed in postprocessing.

A slight shrinkage of the wetted powder materials was observed that affects the geometry of the printed part. As a result, the overall dimensions of the printed parts were 3% lower than the corresponding dimensions of the 3D computer models. Furthermore, this material shrinkage led to a slight curling of the first approximately five layers of the printed compression test parts. Accordingly, these parts offer a convex shape on the bottom side. Figure 5 shows a sintered specimen of the compression test part with a convex lower surface. The figure demonstrates the good preservation of the shape of the test parts, and consequently, that the convex shape is not caused by shrinkage effects due to sintering.

The sintering shrinkage of the compression test parts ranged between 18 and 20%, and showed equal values in every direction. The shape of the compression and the channel test part as well as the inner structure of the channel part could be persevered to a large extent. The structures of the grid test part and the inner channels of the channel test part were only slightly distorted.

The convex bottom surface of the compression test part has been cut to get coplanar planes that were needed for uniaxial compression tests. The mean compression strength

TABLE I. Printing Parameters of the Three Test Parts

Test part	Material	Layer thickness	Printing resolution	Binder solution	Droplet weight
Compression	V5.2	0.3 mm	0.25 mm	14wt%	6.3μg
Channel	V5.2	0.25mm	0.25 mm	14wt%	6.3μg
Grid	V12	0.2 mm	0.2 mm	10wt%	8.2μg

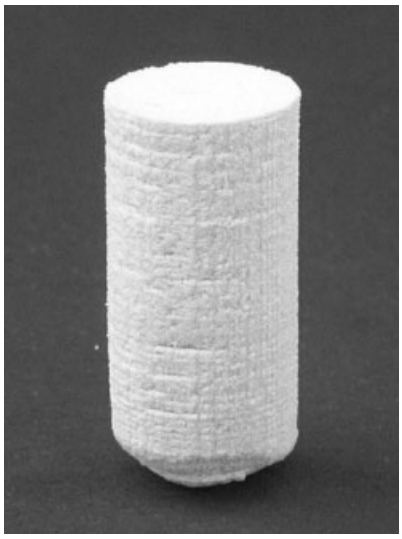

Figure 5. Sintered specimen of the compression test part with convex bottom. The diameter of the part is 11.5 mm.

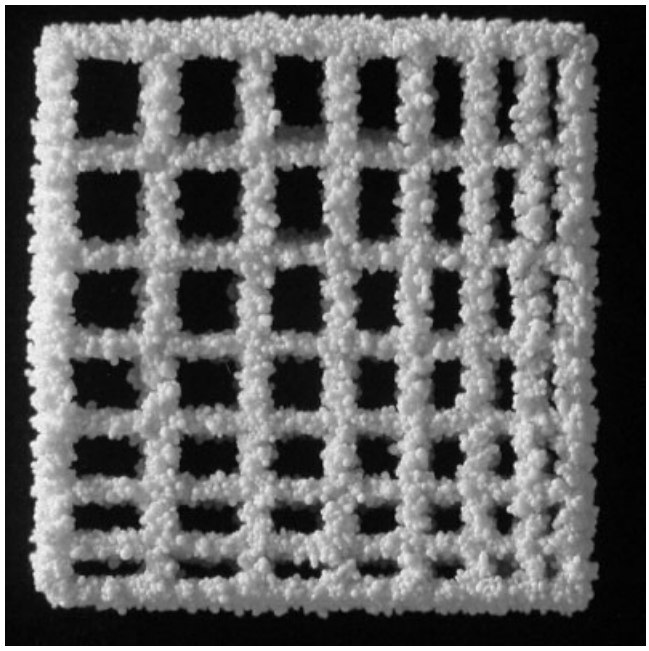

Figure 7. Grid test part with wall thickness of 330 μm. The overall dimensions of the parts are 7.8 $\times$ 7.8 mm^2.

of the sintered compression test parts was measured to 21.2 $\pm$ 2.2 MPa.

Figure 6 shows the structural resolution of the printed channel test part with internal channels. The quadratic cross-section of channels in the z direction is largely preserved with an edge length of 569 $\pm$ 33 μm in the x direction (fast printing axis) and 530 $\pm$ 25 μm in the y direction (slow printing axis). The designed quadratic cross-section of channels in the x and y direction altered into a rectangular shape with a height in the z direction of 447 $\pm$ 37 μm.

The measured wall thickness of the grid test part is 330 $\pm$ 26 μm in the x and y directions (see Figure 7). Some specimens showed a slight distortion of the printed walls. All gaps between the grid walls could be cleaned from unglued powder in post processing.

The typical surface texture of a sintered part is shown in Figure 8. The shape of the powder granules is preserved. Consequently, the surface has a big area and a high surface roughness. There are no sharp edges. The sintering led to a good connection between the particles.

The SEM scan (see Figure 9) of a cross-section of a sintered material (channel test part) shows the pore structure of the bulk material. The pores are in a range between 10 and

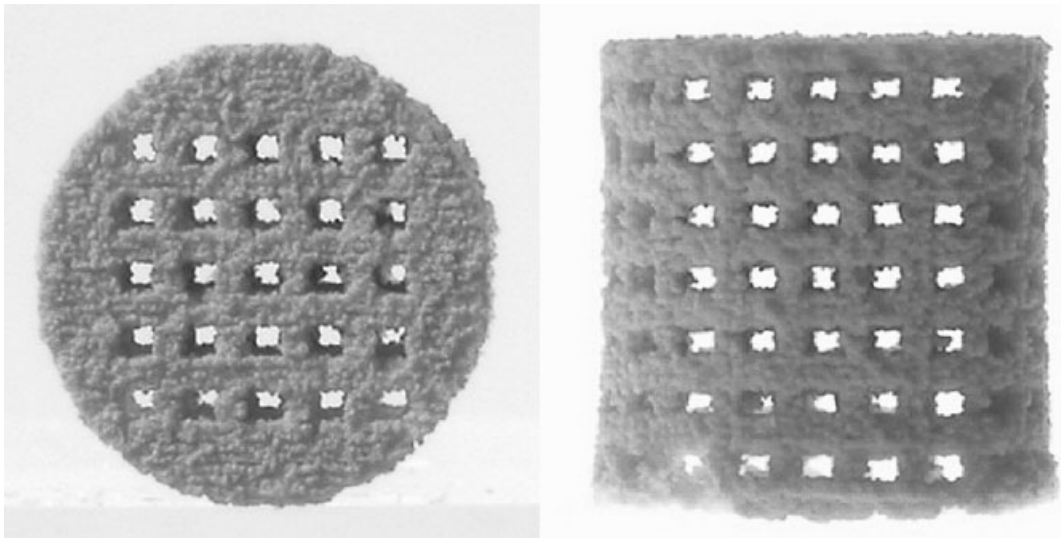

Figure 6. Top view (left) and side view (right) on the sintered channel test part with a diameter of 7.8 mm. The dimensions of the channels range between 447 $\pm$ 37 μm in the z direction and 569 $\pm$ 33 μm in the x direction.

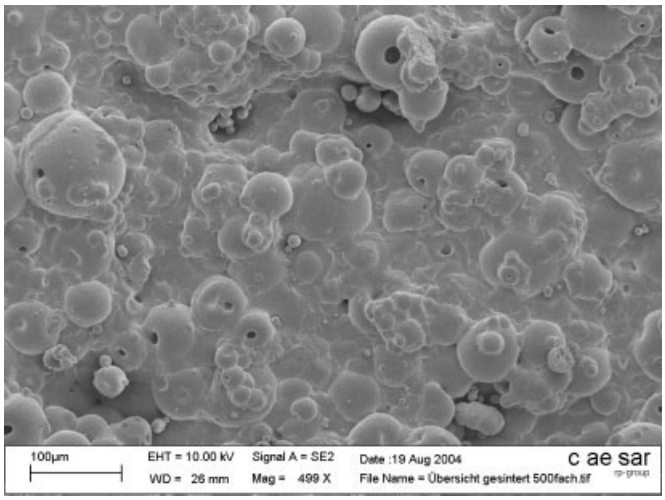

Figure 8. SEM of typical surface texture of a sintered part. The shape of the powder granules is preserved.

30 μm. Figure 9 also demonstrates that the particles had a good connection through sintering. There is a seamless transition between single particles. The contact points of the particles cannot be identified.

DISCUSSION

The manufactured test parts successfully demonstrated the possibility of using the 3D printing process chain to build porous ceramic scaffolds. Previous studies focused on various materials for scaffolds fabricated using 3D printing[7,8] and on the *in vivo* performance of such scaffolds.[9,10,14] The aim of the current study was to investigate the technical potential of a ceramic-based 3D printing process chain for direct fabrication of porous scaffolds with defined inner channels for bone tissue engineering. For bone tissue engineering, interconnecting channels and porosity of the scaffolds are very important. For good osteointegration, a mean pore diameter of 565 μm of inner channels in a scaffold is discussed.[17] The measured channel resolution of the cylindrical test structure with internal channels ranged between 450 and 570 μm, and thus is close to the discussed optimum channel size.

The channel size of the cylindrical test part is almost the same dimension in the x and y directions, whereas the channel size in the z direction is less than the size in x-y direction. This is because the printed binder has to infiltrate the powder deeper than exactly one layer to connect the current layer with the layer underneath. The channel size in the x direction and y direction differs slightly because the droplets cannot be placed that precisely in the bidirectional printing direction x than in the quasi-stationary printing axis y.

The achieved wall thickness of the grid test part down to 330 μm is not sufficient to exactly mimic natural spongiosa of human bone, but is a good structural resolution for the fabrication of highly macroporous scaffolds for tissue engineering applications. Furthermore, all test parts are highly porous because the shape of the ceramic granulates that are used as basic building material was preserved after sintering. The micro- and macroporosity of the scaffolds is supposed to support bone ingrowth[18] as well as to improve the biodegradability of the fabricated scaffolds because of the reduced density of the material itself. Dutta Roy et al.[14] found large amounts of new bone in a 3D printed scaffold that contained pores less than 20 μm in size. The pore size of the scaffolds in the present study was in the range of 10–30 μm. Because the scaffold reported here feature similar surface and porosity to the scaffolds presented in the previous studies,[9,10,19] it is expected that the scaffolds of the present study offer a promising environment for cell adhesion and cell proliferation.

Fragile parts printed in high resolution like the presented test grid part are stable after sintering but cannot be loaded, whereas the channel test part features sufficient stability for usage in tissue engineering applications. Furthermore, the compression test parts show comparable mechanical compression strength to commercial bovine HA bone substitutes.[20] The compression strength of the test parts ranges between that of human spongiosa and that of cortical bone.[21] Consequently, the fabricated ceramic matrices have enough mechanical stability to serve as a scaffold for initial cell attachment and bone tissue engineering and as an implant for bone replacement, but are not suited for carrying high forces in strongly loaded regions in the human skeleton. In this area, an implant provides only low mechanical support for the area to be reconstructed and has to be fixed by metal plates.

Because hydroxyapatite is frequently used as material for bone substitute, it is expected that the scaffold fabricated by the described process chain feature high biocompatiblility. Nevertheless, to ensure the biocompatibility of the ceramic, tests were carried out. 3D test scaffolds have been printed, and cells were seeded on the scaffolds. After the scaffolds were cultivated in a medium, proliferation and viability of the seeded cells were measured. First results show that the new ceramic materials are not toxic and thus well suited for

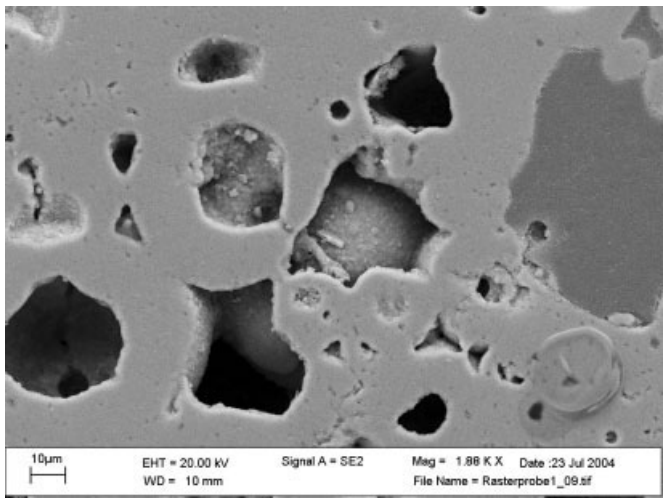

Figure 9. SEM image of a cross-section of a ceramic test part showing the pore structure of the sintered material.

application as custom implants for bone replacement. Detailed results will be published soon (Leukers et al., unpublished). In the future, the osteogenic differentiation capability of human mesenchymal stem cells grown on these scaffolds and the resorbability of the scaffolds will be investigated.

The authors gratefully acknowledge the Friedrich-Baur-Research Institute for Biomaterials, Bayreuth, Germany, for a generous donation of the ceramic powder and Schelofix binder.

REFERENCES

1. Wohlers T. Wohlers report 2004: Rapid prototyping & tooling state of the industry. Fort Collins, CO: Wohlers Associates; 2004.
2. Yang A, Leong KF, Du Z, Chua CK. The design of scaffolds for use in tissue engineering. Part II. Rapid prototyping techniques. Tissue Eng 2002;8:1–11.
3. Cooke MN, Fisher JP, Dean D, Rimnac C, Mikos AG. Use of Stereolithography to manufacture critical-sized 3D biodegradable scaffolds for bone ingrowth. J Biomed Mater Res Part B: Appl Biomater 2002;64B:65–69.
4. Hutmacher DW, Schantz JT, Zein I, Ng KW, Tan KC, Teoh SH. Mechanical properties and cell cultural response of polycaprolactone scaffolds designed and fabricated via fused deposition modeling. J Biomed Mater Res 2001;55:203–216.
5. Landers R, Mülhaupt R. Desktop manufacturing of complex objects, prototypes and biomedical scaffolds by means of computer-assisted design combined with computer-guided 3D plotting of polymers and reactive oligomers. Macromol Mater Eng 2000;282:17–21.
6. Ang TH, Sultana FSA, Hutmacher DW, Wong YS, Fuh JYH, Mo XM, Loh HT, Burdet E, Teoh SH. Fabrication of 3D chitosan-hydroxyapatite scaffolds using a robotic dispensing system. Mater Sci Eng C 2002;20:35–42.
7. Park A, Wu B, Griffith LG. Integration of surface modification and 3D fabrication techniques to prepare patterned poly(L-lactide) substrates allowing regionally selective cell adhesion. J Biomater Sci Polym Edn 1998;9:89–110.
8. Lam CXF, Mo XM, Teoh SH, Hutmacher DW. Scaffold development using 3D printing with a starch-based polymer. Mater Sci Eng C 2002;20:49–56.
9. Simon JL, Dutta Roy T, Parsons JR, Rekow ED, Thompson VP, Kemnitzer J, Ricci JL. Engineered cellular response to scaffold architecture in a rabbit trephine defect. J Biomed Mater Res 2003;66A:275–282.
10. Dutta Roy T, Simon JL, Ricci JL, Rekow ED, Thompson VP, Parsons JR. Performance of degradable composite bone repair products made by three-dimensional fabrication techniques. J Biomed Mater Res 2003;66A:283–291.
11. Steidle C, Klosterman D, Chartoff R, Graves G, Osborne N. Automated fabrication of custom bone implants using rapid prototyping. Proceedings of the 44th International SAMPE Symposium and Exhibition, Long Beach, CA, May 1999.
12. Lee G, Barlow JW, Fox WC, Aufdlemorte TB. Biocompatibility of SLS-formed Calcium Phosphate Implants. Proceedings of the Solid Freeform Fabrication Symposium, Austin, Texas; 1996. p 15–21.
13. Chu T-MG, Halloran JW, Hollister SJ, Feinberg SE. Hydroxyapatite implants with designed internal architecture. J Mater Sci Mater Med 2001;12:471–478.
14. Dutta Roy T, Simon JL, Ricci JL, Rekow ED, Thompson VP, Parsons JR. Performance of hydroxyapatite bone repair scaffolds created via three-dimensional fabrication techniques. J Biomed Mater Res 2003;67A:1228–1237.
15. Wilson CE, de Bruijn JD, von Blitterswijk CA, Verbout AJ, Dhert WJA. Design and fabrication of standardized hydroxyapatite scaffolds with a defined macro-architecture by rapid prototyping for bone-tissue-engineering research. J Biomed Mater Res 2004;68A:123–132.
16. Taboas JM, Maddox RD, Krebsbach PH, Hollister SJ. Indirect solid free form fabrication of local and global porous, biomimetric and composite 3D polymer–ceramic scaffolds. Biomaterials 2003;24:181–194.
17. Gauthier O, Bouler J-M, Aguado E, Pilet P, Daculsi G. Macroporous biphasic calcium phosphate ceramics: Influence of macropore diameter and macroporosity percentage on bone ingrowth. Biomaterials 1998;19:133–139.
18. Weiss P, Obadia L, Magne D, Bourges X, Rau C, Weitkamp T, Khairoun I, Bouler JM, Chappard D, Gauthier O, Daculsi G. Synchrotron X-ray microtomography (on a micron scale) provides three-dimensional imaging representation of bone ingrowth in calcium phaspate biomaterials. Biomaterials 2003;24:4591–4601.
19. Melican MC, Zimmerman MC, Dhillon MS, Ponnambalam AR, Curodeau A, Parsons JR. Three-dimensional printing of porous metallic surfaces: A new orthopaedic application. J Biomed Mater Res 2001;55:194–202.
20. Charriere E, Lemaitre J, Zysset, P. Hydroxyapatite cement scaffolds with controlled macroporosity: fabrication protocol and mechanical properties. Biomaterials 2003;24:809–817.
21. An YH. Mechanical properties of bone. In: An YH, Draughn RA, eds. Mechanical testing of bone and the bone–implant interface. Boca Raton, FL: CRC Press; 2000. p 41–63.